Model for Pressure Drop Hysteresis in Trickle-Beds

C. F. Chu
K. M. Ng
Department of Chemical Engineering
University of Massachusetts
Amherst, MA 01003

A large number of empirical correlations are available for predicting pressure drop in trickle beds (Gianetto et al., 1978). For a given gas and liquid flow rate, a single value of the pressure gradient can be estimated. It has gradually become clear, however, that the pressure gradient might not be unique and multiple hydrodynamic states can exist in the trickling flow regime. Kan and Greenfield (1978) observed that the pressure gradient at a specific gas and liquid flow rate depends on how that state is reached. To be more specific, a hysteresis loop with an upper and lower branch bounds all possible pressure gradients or hydrodynamic states for a fixed gas (liquid) flow rate, while varying the liquid (gas) flow rate. Intermediate pressure gradients within the loop can be obtained by increasing and decreasing the liquid (gas) flow rate between the two end points of the loop. These observations have since then been confirmed in the studies of Levec et al. (1986), Christensen et al. (1986), and Levec et al. (1988).

The experimental studies carried out by the previously-mentioned researchers and in our laboratory show the following particle-level phenomenon. Along the lower branch, the liquid is primarily in the form of liquid filaments. As depicted in Figure 1a, these are liquid streams that flow down the column in the channels between the packings. The particles are, of course, in contact but are represented as isolated circles in this schematic. A filament is more or less aligned along the vertical direction, and its width can extend over several pore chambers. In increasing the liquid flow rate to the trickling-pulsing flow transition point, i.e., the upper end-point of the hysteresis loop, this flow pattern is disrupted and the entire bed is wetted by liquid. If the liquid flow rate is reduced at this point, the liquid is primarily in the form of liquid films due to the vigorous mixing earlier, while the gas flows in the remaining void space (Figure 1b). This leads to a larger amount of gas-liquid interfacial interactions than liquid filaments and results in a higher-pressure gradient along the upper branch. This higher-pressure gradient, in turn, sustains the films and prevents them from reverting back to filaments.

Correspondence concerning this paper should be addressed to K. M. Ng.

This work was carried out to quantitatively investigate the pressure drop-liquid distribution relationship for a trickle-bed packed with equal-sized spheres, so that it supports the qualitative observations. A number of theoretical studies on gas-liquid two-phase trickling flow in trickle beds have appeared in the literature. For instance, Saez et al. (1986) modeled the packed bed as a bundle of parallel, cylindrical or constricted tubes, in which annular gas-liquid flow takes place. A similar study by Biswas et al. (1988) is limited to cylindrical tubes but allows stratified flow, where part of the channel wall is in contact with the gaseous phase. Because trickle-beds are actually made up of interconnected channels among the packed particles, this study begins with a porous medium model.

Bicontinuous Porous Medium Model

A wide variety of porous medium models have been proposed for studying flow in porous media (van Brakel, 1975). In general, emphasis is placed either on the pore space such as flow over a network of interconnected constricted tubes (Payatakes et al., 1980) or on the solid matrix such as flow over an array of solid cylinders or spheres (Kuwabara, 1959). For gas-liquid flow in trickle beds, the liquid tends to flow downwards from particle to particle, particularly under the condition of film flow. The gas is less influenced by gravity and does not follow the path taken by the liquid. In this case, it is necessary to consider the following bicontinuous model which allows easy implementation of a two-phase flow analysis.

It is basically a regular cubic packing of equal-sized spheres. However, the packing is oriented, or tilted, in such a way that if viewed from above, each sphere rests on top of three other spheres spaced evenly apart. Figure 2 shows three layers of such a tilted cubic packing as viewed from above. Spheres on the top layer are marked by dotted lines, the second layer by solid lines, and the third by heavy solid lines. This three-layer configuration can be repeated indefinitely into the paper to yield a packing of any height. In addition, the tilted cubic packing is periodic along its four edges; for instance, sphere C actually rests on G, H and I, while B is on H, J, K and so on.

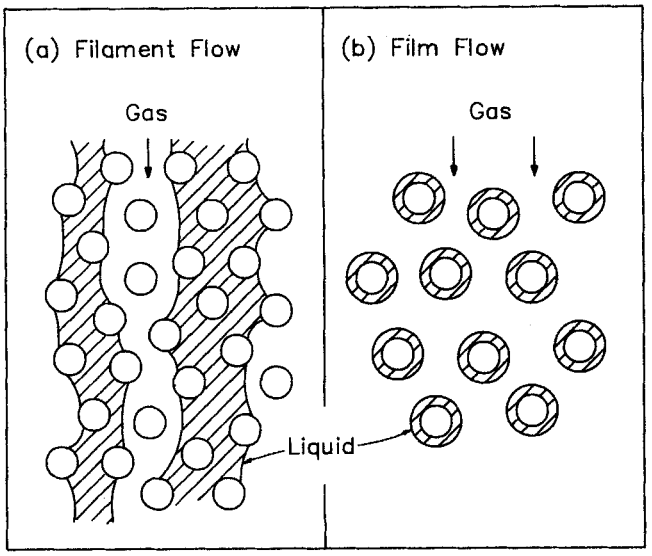

Figure 1. Idealization of the flow patterns in the trickling flow regime: a) filament flow; b) film flow.

A tilted cubic network of flow channels is embedded within the tilted cubic packing of spheres (Figure 3). To understand the network structure, consider first the cluster of spheres in Figure 2: A on the top level; D, E and F on the second; L, M and N on the third; and A′ is on the fourth directly under A. There are three channels bounded by spheres ADFN, ADEL, and AEFM leading into the pore chamber bounded by spheres ADEFLMNA′. This pore chamber is represented as a dotted circle, A, in Figure 3, and clearly there is a pore chamber immediately under every sphere. The three channels are marked as 1, 2 and 3, respectively, leading into pore chamber A. Similarly, there are three channels coming out of pore chamber A bounded by spheres A′DLN, A′ELM, and A′FMN (Figure 2), which are labelled as 4, 5 and 6, respectively, in Figure 3. Note that branches 4, 5 and 6 connect pore chamber A to pore chambers D, E and F, respectively.

It should be clear by now that the topology of the tilted cubic network of flow channels is identical to that of the tilted cubic packing. Each has a coordination number of six. Now, let us assume that the tilted cubic packing is twisted around in such a way that the topology remains the same but the size distribution

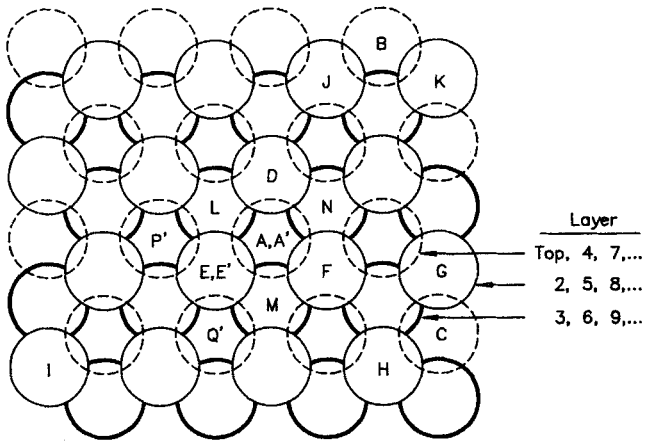

Figure 2. Top view of a tilted cubic packing.

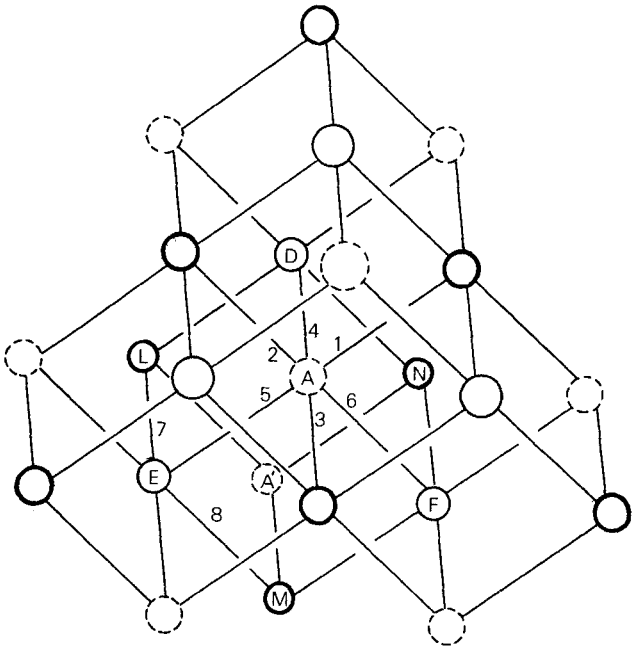

Figure 3. A tilted cubic network of flow channels.

of the flow channels corresponds to what one finds in an actual random sphere pack. This is achieved by randomly assigning a size to each and every channel in the network using the constriction-size distribution obtained from a computer-generated sphere pack (Chan and Ng, 1986, 1988). For simplicity, we further assume that the flow channels are cylindrical capillary tubes and have the same length. As shown in Payatakes et al. (1973, 1980), the appropriate length for a random bed packed with equal spheres is the length of periodicity, l, defined as

$$l = \left(\frac{\pi}{6(1-\epsilon)} \langle d_g^3 \rangle \right)^{1/3} \tag{1}$$

where d_g is the particle diameter. If all the particles are of exactly the same size and the porosity, ϵ, is 0.4, l is equal to 0.9556 of d_g.

Liquid Distribution and Flow Analysis

Annular flow

As discussed previously, the upper branch of the hysteresis loop corresponds to film flow, in which all the spherical particles are assumed to be covered by liquid films, while the gas flows in the remaining void space. In this case, we can model it as gas-liquid annular flow in the flow channel network. Figure 4 shows such a channel of diameter D, inclined at an angle of α to the horizontal plane. For the tilted cubic network, α equals $\sin^{-1}(\sqrt{3})$. Following the approach of Taitel and Dukler (1976), we obtain from momentum balance for each phase.

$$-A_l \frac{dp}{dz} - \tau_{wl} S_l + \tau_i S_i + \rho_l A_l g \sin \alpha = 0 \tag{2}$$

$$-A_g \frac{dp}{dz} - \tau_i S_i + \rho_g A_g g \sin \alpha = 0 \tag{3}$$

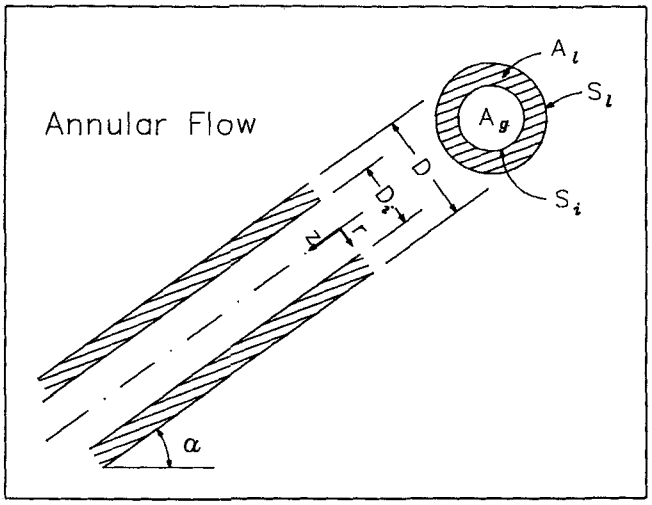

Figure 4. Inclined flow channel with annular flow.

where A_l and A_g are the cross-sectional flow areas for liquid and gas, respectively. And, S_l and S_i are the liquid-wall and gas-liquid interfacial lengths, respectively. The shear stress at the gas-liquid interface, τ_i, and that at the wall, τ_{wl}, can be evaluated with the following correlations

$$\tau_{wl} = C_l \left(\frac{D_l u_l}{\nu_l}\right)^{-n} \frac{\rho_l u_l^2}{2}, \quad D_l = \frac{4A_l}{S_l} \tag{4}$$

$$\tau_i = C_g \left(\frac{D_g u_g}{\nu_g}\right)^{-n} \frac{\rho_g u_g^2}{2}, \quad D_g = \frac{4A_g}{S_i} \tag{5}$$

where u_l and u_g are the average velocity in the liquid and gaseous phases, respectively,

$$u_l = q_l/A_l \qquad u_g = q_g/A_g \tag{6}$$

For laminar flow, $C_l = C_g = 16$ and $n = 1.0$.

For the upper branch, we assume that the liquid is evenly distributed within the bed. Thus, each spherical particle or each flow channel receives the same amount of liquid flow. The corresponding gas flow rates in the channels can differ and, in general, the gas flow rate is smaller in a narrower channel. The diameter of the gas core also varies from channel to channel. Therefore, for a given pressure gradient, both gas flow rate, q_g, and gas core diameter, D_i, have to be determined simultaneously for each and every channel in the tilted cubic network. This can be accomplished as follows.

Elimination of $\tau_i S_i$ from Eqs. 2 and 3, and substitution of Eqs. 4 and 6 into the resulting equation, we get,

$$-\frac{dp}{dz} = \frac{C_l \left(\frac{4q_l}{\nu_l S_l}\right)^{-n} \frac{\rho_l}{2}\left(\frac{q_l}{A_l}\right)^2 - (\rho_l A_l + \rho_g A_g) g \sin\alpha}{A_l + A_g} \tag{7}$$

With

$$A_l = \pi(D - D_i)^2/4 \qquad A_g = \pi D_i^2/4$$

$$S_l = \pi D \qquad S_i = \pi D_i \tag{8}$$

we can see that the righthand side of Eq. 7 depends only on D_i. Likewise, Eq. 3 can be rewritten as,

$$q_g = \left\{\left[-A_g \frac{dp}{dz} + \rho_g A_g g \sin\alpha\right] \Big/ \left[C_g \left(\frac{4}{\nu_g S_i}\right)^{-n} \frac{\rho g}{2A_g^2}\right]\right\}^{1/(2-n)} \tag{9}$$

If $(-dp/dz)$ for a flow channel is assumed, we can calculate D_i from Eq. 7 using any numerical search technique. Then, q_g can be calculated from Eq. 9. At each junction or node of the network, we require that the summation of the six gas flow rates be zero,

$$\sum_{i=1}^{6} q_{g,i} = 0 \tag{10}$$

The actual calculations were carried out with an IMSL subroutine ZSPOW for the solution of a system of nonlinear equations. For a given pressure drop across the network, the pressure values of the nodes at the top and bottom were fixed. After making an initial guess of the pressures at the internal nodes, these pressures were iterated until Eq. 10 was satisfied.

Two complications can arise:

1. The calculated ratio of gas core to tube diameter ($\kappa = D_i/D$) can be very small for some flow channels and the existence of annular flow is questionable. We assume that if κ is less than 0.4, i.e., if 86% of the cross-section is liquid-filled, the channel is clogged by liquid, and the Poiseuille equation for single-phase flow replaces the two-phase flow equations in the continuation of iteration.

2. Although the liquid phase is found to always flow down an inclined tube under the usual conditions for trickling flow, the gas phase can flow up in the event that, because of the network effect (Ng and Payatakes, 1985), the pressure at the lower end is higher than that at the higher end of the tube. Equations 2 and 3, however, are still valid for this situation of countercurrent flow, and no change is needed in the calculations.

Segregated flow

The lower branch of the hysteresis loop corresponds to filament flow. To visualize such an isolated filament surrounded by gas, consider that liquid is injected to sphere A such that it is completely wetted. In other words, channels 1, 2, 3 and 4, 5, 6 are completely filled (Figure 3). To be specific, consider channel 5. At this point, it branches out into channels 7 and 8, which are bounded by spheres A'E'P'L and A'E'Q'M, respectively (Figure 2). Spheres P' and Q' are on the same level as A'. Because the liquid in one channel is split to flow to two channels, either is completely filled. Further observation reveals that this pattern of three-filled, three-filled, six-partially-filled channels repeats itself as one moves down the network, again allowing convenient programming. This particular filament will be referred to as a monofilament, implying that it is started with one completely-wetted sphere. We can have a bifilament by starting with two spheres on the same layer, trifilament with three, and so on.

Thus, a flow channel can be either gas- or liquid-filled, or has segregated flow. The Poiseuille equation is used for single-phase gas or liquid flow in a channel. Figure 5 shows a schematic of an inclined channel with segregated flow. A momentum balance for each phase yields,

$$-A_l \frac{dp}{dz} - \tau_{wl} S_l + \tau_i S_i + \rho_l A_l g \sin\alpha = 0 \tag{11}$$

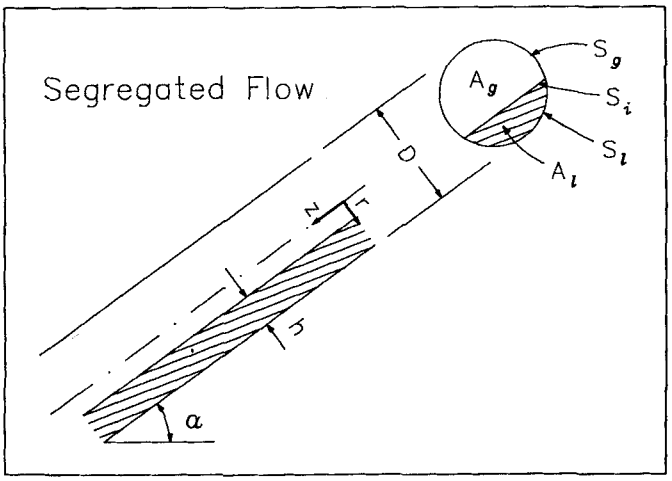

Figure 5. Inclined flow channel with segregated flow.

$$-A_g \frac{dp}{dz} - \tau_{wg} S_g - \tau_i S_i + \rho_g A_g g \sin \alpha = 0 \qquad (12)$$

Equation 4 can still be used to evaluate τ_{wl} in Eq. 11. As discussed in Taitel and Dukler (1976), since the gas velocity u_g is generally much higher than that at the gas-liquid interface, we have

$$\tau_{wg} \doteq \tau_i = C_g \left(\frac{D_g u_g}{\nu_g}\right)^{-n} \frac{\rho_g u_g^2}{2}, \quad D_g = \frac{4A_g}{S_g + S_i} \qquad (13)$$

Equations 11 and 12 can be solved for the entire network with the same procedure for film flow. Instead of D_i, the height of the film h is allowed to vary in all the channels with segregated flow. Note that A_l, A_g, S_l, S_g, and S_i can all be expressed in terms of h.

Results and Discussion

To confirm the validity of our proposed physical picture and the flow analysis, results are generated for comparison with available experimental data. Shown in Figure 6 with solid lines is the experimental pressure gradient hysteresis loop at a fixed superficial gas mass flow rate of 756 kg/m^2 · h (Christensen et al., 1986). The simulation data of the upper branch for L = 1, 2, 3, 3.5 × 10^4 kg/m^2 · h are indicated with circles. The calculational procedure begins with given L and $|\nabla p|$, and then the gas flow rate, G, is calculated. Subsequently, $|\nabla p|$ was iterated a few times to obtain the pressure gradient corresponding to G = 756 kg/m^2 · h. All the simulation data points are based on a 6 × 6 × 6 tilted cubic sphere packing: there are six layers with 36 spheres on each layer. Also, each data point at a fixed liquid flow rate is the mean value of four different realizations, each of which involves a different network assigned randomly with sizes according to the same constriction-size distribution. The error bar indicates the scatter in the simulation data.

The simulation data for the lower branch are also indicated in Figure 6, which also shows reasonable agreement with experimental data. As for the upper branch, we again iterated a few times on $|\nabla p|$ to obtain the pressure gradient corresponding to G = 756 kg/m^2 · h. The major difference is that we have to assume the liquid distribution before starting the calculations:

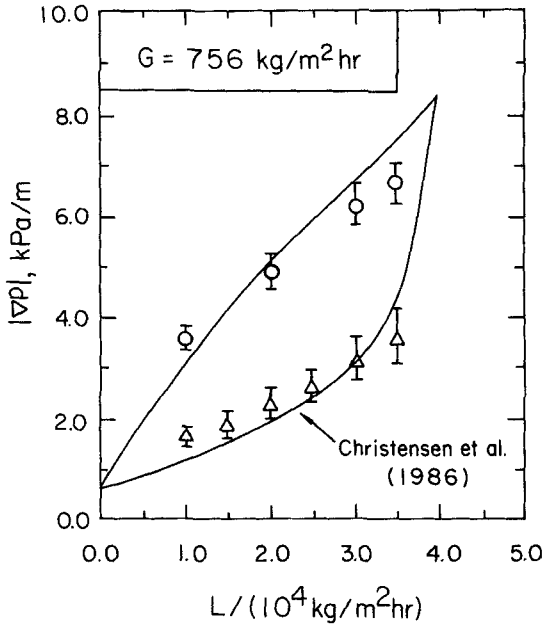

Figure 6. Theory vs. experiment for pressure gradient hysteresis.

i.e., we have to specify the number of monofilaments, bifilaments, etc., as well as their locations in the network. This poses a question. How do we know that the assumed liquid distribution is a reasonable one? We propose that the average film thickness for all the channels with segregated flow, $\langle h/D \rangle$ has to be close to 0.5. If the average film thickness is too large, a monofilament, for instance, would expand to become a bifilament under the given operating conditions; on the other hand, if the average film thickness is too small, a wide filament would contract to a narrower one.

Each data point for the lower branch is the mean value of a number of realizations and involves two different networks assigned randomly with sizes according to the same constriction-size distribution. Different flow configurations, i.e., the number and locations of the monofilaments, bifilaments, etc., can yield $\langle h/D \rangle$ close to 0.5, and a slightly different $|\nabla p|$ for a given L and G = 756 kg/m^2 · h. The variations are reflected in the upper and lower bounds for each data point. We found, however, that the different flow configurations which provide a $\langle h/D \rangle$ value close to 0.5 for a given liquid flow rate have the following common feature. The filaments irrespective of the number and sizes occupy an approximately constant fraction of the sphere pack cross-section. The fraction increases with the

Table 1. Dependence of the Fraction of the Sphere Pack Cross-Section Occupied by Liquid Filaments on Liquid Flow Rate*

L, kg/m^2 · h	Fraction
10,000	0.19
15,000	0.28
20,000	0.38
25,000	0.45
30,000	0.55
35,000	0.58

*G = 756 kg/m^2 · h

Table 2. Effect of the Critical κ on the Pressure Gradient and the Fraction of Channels Clogged by Liquid

$\kappa (=D_i/D)$	$\lvert\nabla p\rvert$, kPa/m	Fraction of Channels Clogged by Liquid
0.2	5.1	0.17
0.3	5.1	0.19
0.4	5.1	0.24
0.5	5.2	0.31

Table 3. Effect of Packing Size on Pressure Gradient

Packing Size	$\lvert\nabla p\rvert$, kPa/m
$4 \times 4 \times 6$	5.2
$6 \times 6 \times 6$	5.1
$8 \times 8 \times 6$	4.9
$6 \times 6 \times 4$	4.6
$6 \times 6 \times 8$	5.2
$6 \times 6 \times 10$	5.2
$8 \times 8 \times 10$	5.0

liquid flow rate (Table 1). This confirms the experimental data that liquid holdup increases with liquid flow rate (Christensen et al., 1986; Levec et al., 1988). We should point out that Christensen et al. postulated that filaments are gradually replaced by films along the lower branch as the liquid flow rate is increased. Based on our analysis, the filament fraction does not necessarily decrease as transition to pulsing is approached.

Finally, two points regarding the upper branch in Figure 6 need to be discussed. We assumed that, if $\kappa(=D_i/D)$ for a flow channel is less than 0.4, the channel is clogged by liquid. Table 2 shows the impact of this *ad hoc* assumption on $\lvert\nabla p\rvert$ at $L = 20{,}000\ \mathrm{kg/m^2 \cdot h}$ and $G = 756\ \mathrm{kg/m^2 \cdot h}$ is minimal. Also shown for each critical κ is the fraction of channels clogged by liquid, which obviously increases with the critical κ. Furthermore, we pointed out that the data for the upper branch are all based on $6 \times 6 \times 6$ tilted cubic sphere packs. The effect of packing size on $\lvert\nabla p\rvert$ at $L = 20{,}000\ \mathrm{kg/m^2 \cdot h}$ and $G = 756\ \mathrm{kg/m^2 \cdot h}$ is examined in Table 3. The impact is small as we change the cross-sectional area, the packing length, or the overall size.

Notation

A = cross-sectional area
C = coefficient
D = diameter
d_g = particle diameter
G = superficial mass flow rate of gas
g = acceleration due to gravity
h = thickness of liquid film in Figure 5
i = dummy index
L = superficial mass flow rate of liquid
l = length of periodicity
n = exponent
p = pressure
q = volumetric flow rate
r = radial coordinate
S = length of an interface
u = mean velocity
z = axial coordinate

Greek letters

α = angle of inclination as measured from a horizontal plane
ϵ = porosity
κ = ratio of gas core to tube diameter
ν = kinematic viscosity
ρ = density
τ = shear stress

Subscripts

g = gas
i = gas-liquid interface
l = liquid
w = wall

Literature Cited

Biswas, J., G. V. Bhaskar, and P. F. Greenfield, "Stratified Flow Model for Two-Phase Pressure Drop Prediction in Trickle Beds," *AIChE J.*, **34,** 510 (1988).

Chan, S. K., and K. M. Ng, "Geometrical Characteristics of a Computer-Generated Three-Dimensional Packed Column of Equal and Unequal Sized Spheres—With Special Reference to Wall Effects," *Chem. Eng. Comm.*, **48,** 215 (1986).

Chan, S. K., and K. M. Ng, "Geometrical Characteristics of the Pore Space in a Random Packing of Equal Spheres," *Powder Tech.*, **54,** 147 (1988).

Charpentier, J. C., and M. Favier, "Some Liquid Holdup Experimental Data in Trickle-Bed Reactors for Foaming and Nonfoaming Hydrocarbons," *AIChE J.*, **21,** 1213 (1975).

Christensen, G., S. J. McGovern, and S. Sundaresan, "Cocurrent Downflow of Air and Water in a Two-Dimensional Packed Column," *AIChE J.*, **32,** 1677 (1986).

Gianneto, A., G. Baldi, V. Specchia, and S. Sicardi, "Hydrodynamics and Solid-Liquid Contacting Effectiveness in Trickle-Bed Reactors," *AIChE J.*, **24,** 1087 (1978).

Kan, K. M., and P. F. Greenfield, "Multiple Hydrodynamic States in Cocurrent Two-Phase Downflow through Packed Beds," *Ind. Eng. Chem. Process Des. Dev.*, **17,** 482 (1978).

Kuwabara, S., "The Forces Experienced by Randomly Distributed Parallel Circular Cylinders or Spheres in a Viscous Flow at Small Reynolds Numbers," *J. Phys. Soc. Japan*, **14,** 527 (1959).

Levec, J., K. Grosser, and R. G. Carbonell, "The Hysteretic Behavior of Pressure Drop and Liquid Holdup in Trickle Beds," *AIChE J.*, **34,** 1027 (1988).

Levec, J., A. E. Saez, and R. G. Carbonell, "The Hydrodynamics of Trickling Flow in Packed Beds. Part II: Experimental Observations," *AIChE J.*, **32,** 369 (1986).

Ng, K. M., and A. C. Payatakes, "Critical Evaluation of the Flow Rate—Pressure Drop Relation Assumed in Permeability Models," *AIChE J.*, **31,** 1569 (1985).

Payatakes, A. C., K. M. Ng, and R. W. Flumerfelt, "Oil Ganglion Dynamics During Immiscible Displacement: Model Formulation," *AIChE J.*, **26,** 430 (1980).

Payatakes, A. C., C. Tien, and R. M. Turian, "A New Model for Granular Porous Media," *AIChE J.*, **19,** 58 (1973).

Saez, A. E., R. G. Carbonell, and J. Levec, "The Hydriodynamics of Trickling Flow in Packed Beds: Part II. Conduit Models," *AIChE J.*, **32,** 353 (1986).

Taitel, Y., and A. E. Dukler, "A Model for Predicting Flow Regime Transitions in Horizontal and Near Horizontal Gas-Liquid Flow," *AIChE J.*, **22,** 47 (1976).

van Braker J., "Pore Space Models for Transport Phenomena in Porous Media—Review and Evaluation with Special Emphasis on Capillary Liquid Transport," *Powder Tech.*, **11,** 205 (1975).

Manuscript received June 24, 1988, and revision received May 15, 1989.